Available at www.sciencedirect.com

ScienceDirect

journal homepage: www.elsevier.com/locate/he

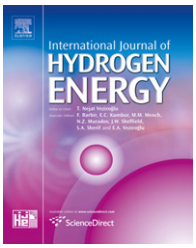

Electrochemical investigations on cobalt-microencapsulated $MmNi_{2.38}Al_{0.82}Co_{0.66}Si_{0.77}Fe_{0.13}Mn_{0.24}$ hydrogen storage alloys for Ni–MH batteries

K. Manimaran [a,*], M.V. Ananth [a], M. Raju [a], N.G. Renganathan [b], M. Ganesan [a], G. Nithya [c]

[a] Central Electrochemical Research Institute, (CECRI), Karaikudi 630006, Tamil Nadu, India
[b] Vel Tech University, Chennai 600062, Tamil Nadu, India
[c] Dhanalakshmi Srinivasan College of Arts and Science for Women, Perambalur 621212, Tamil Nadu, India

ARTICLE INFO

Article history:
Received 2 July 2009
Received in revised form
24 December 2009
Accepted 9 February 2010
Available online 24 March 2010

Keywords:
Activation energy
Exchange current density
$MmNi_5$
State-of-charge

ABSTRACT

Cobalt coatings were applied over lanthanum process-rich $MmNi_{2.38}Al_{0.82}Co_{0.66}Si_{0.77}Fe_{0.13}Mn_{0.24}$ alloy particles by an autocatalytic electroless deposition process. Electrode characteristics such as electrochemical capacity and cycle life were studied for the uncoated and coated alloys. The structure and morphology of the surface modified samples were characterized with XRD and SEM/EDAX techniques. The cobalt coating forms a thin layer on the surface of the core material and the coated alloys exhibit a 15% improvement in performance over the bare alloy. A comparison of the electrochemical impedance behaviour of the bare and cobalt-coated metal hydride electrodes at different states-of-charge reveals that the relaxation period is distinct for different SOCs. The cobalt microencapsulations influence the apparent activation energy of the dehydriding process. The calculated equivalent rate constant (k_{eq}) values confirm the improvement in reversibility for the cobalt-coated alloy as compared to the bare alloy.

1. Introduction

Nickel–metal hydride (Ni–MH) batteries are in widespread use by virtue of their higher energy density and superior rate capabilities as compared to the conventional nickel–cadmium batteries [1]. The performance of the system is governed by the electrochemical activity of the MH negative electrode. Different types of hydrogen storage alloys (AB, AB_2, A_2B, AB_5, etc.) have been investigated as anode active materials in Ni–MH batteries. Many manufacturers prefer the AB_5 type alloys. $LaNi_5$ is a promising hydrogen storage material for such applications [2]. $LaNi_5$-based alloys exhibit longer cycle life though their capacity is inferior to that of AB_2 type alloys [3]. Particle disintegration due to pulverization and surface oxidation are responsible for the capacity fade observed in $LaNi_5$-based alloys during cycling. It has been demonstrated that cobalt as an additive can enhance the long-term stability of MH electrodes [4]. Nowadays, misch metal-based AB_5 type alloy formulations are preferred for such applications. Among the various factors that can influence the properties, lanthanum/cerium ratio has a significant role on the electrochemical hydrogen storage [5].

The performance of the metal hydride electrode is dictated by the kinetics of the redox reactions occurring at the electrode–electrolyte interface during the hydriding/dehydriding processes. Kinetic parameters of the redox reactions have

* *Corresponding author*. Tel.: +91 4565 227550; fax: +91 4565 227713.
E-mail address: manimaran@ymail.com (K. Manimaran).
0360-3199/$ – see front matter © 2010 Professor T. Nejat Veziroglu. Published by Elsevier Ltd. All rights reserved.
doi:10.1016/j.ijhydene.2010.02.045

Table 1 – Bath composition and process of electroless deposition for cobalt microencapsulation.

Composition	Content ($g l^{-1}$)
Cobalt sulphate heptahydrate	32
Sodium hypophosphite	20
Sodium citrate	84
Ammonium chloride	50
pH	9
Temperature (°C)	90

been determined by several electroanalytical techniques [6–10]. Electrochemical studies on $La_{0.7}Mg_{0.3}Ni_{3.4-x}Co_{0.6}Mn_x$ alloy have been reported by Liu et al. [11]. Absorption and desorption of hydrogen at the metal–electrolyte interface have been investigated by electrochemical impedance spectroscopy (EIS) and cyclic voltammetry, and the results indicate that these processes are markedly suppressed in an electrolyte of NaOH as compared to in KOH [10]. Darowicki and Slepski [12] carried out an *in situ* EIS study of MH electrode reactions. The state-of-charge (SOC) of Ni–MH batteries have also been investigated by EIS [13]. Raju et al. [7] analyzed the kinetic parameters of the MH electrode using EIS. Haran et al. [14] derived the exchange current density values from the polarization measurements.

The effect of surface modification on the electrochemical performance of $LaNi_5$-based hydrogen storage alloys in Ni–MH batteries has been reported by Deng et al. [15]. Electroless

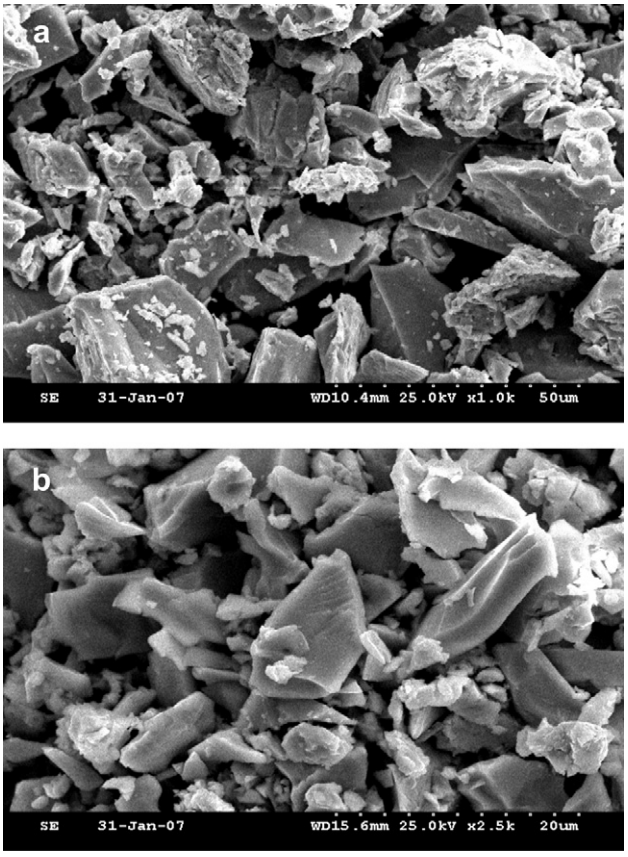

Fig. 1 – SEM images of (a) bare and (b) Co-coated MH alloy particles.

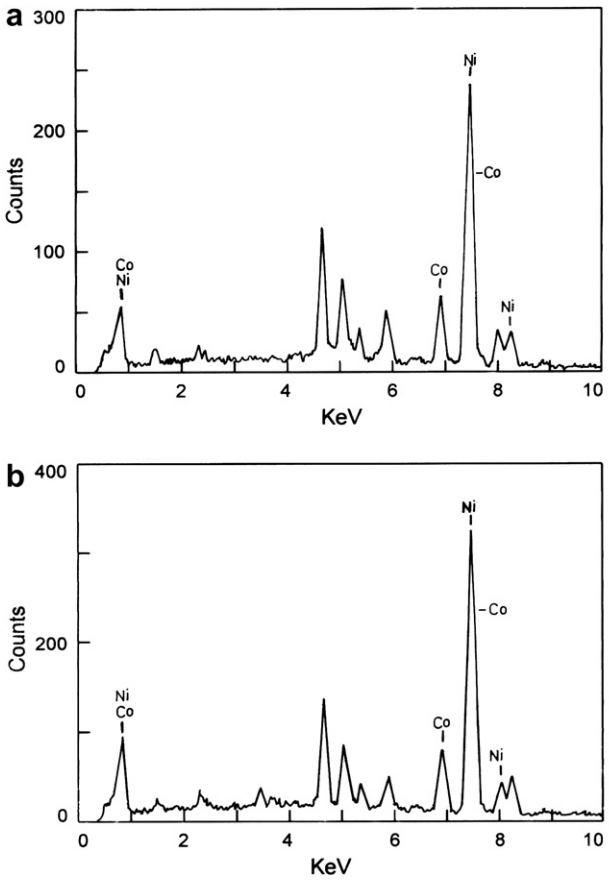

Fig. 2 – EDAX spectrum of (a) bare and (b) Co-coated MH alloy particles.

coatings of Cu, Ni–P, Ni–B, Pd and Co over metal hydride alloy particles have been shown to bestow improvement in cycle life and high rate capability [16–19]. Cobalt encapsulation over the alloy particles by electroless deposition provides an oxidized surface [20] that enhances the electronic conductivity, thereby increasing charge efficiency. The cobalt coating intensifies the catalytic reactions during charge–discharge as well as during overcharge by suppressing the hydrogen evolution. Partial substitution of cobalt for nickel in the MH alloy particles has also been found to be beneficial [21] in reducing volume

Table 2 – Elemental composition in weight percent of bare and Co-coated MH alloy as obtained from EDAX.

Element	Bare MH alloy (%)	Co-coated MH alloy (%)
La	31.36	27.99
Ce	3.36	1.87
Ni	47.48	53.00
Al	2.08	1.41
Co	10.12	10.94
Si	0.03	0.13
Fe	0.35	0.49
Mn	5.22	4.17
Total	100.00	100.00

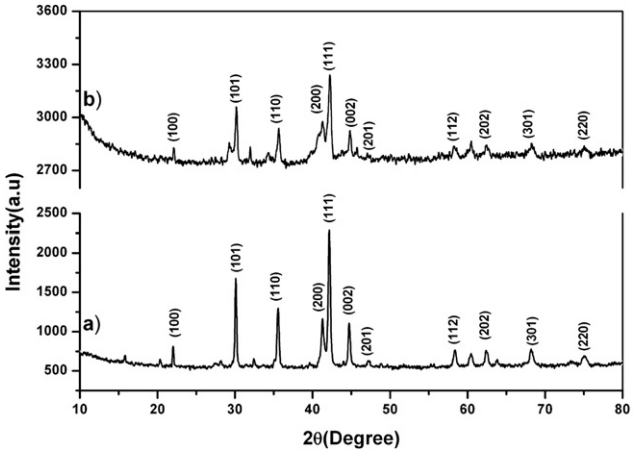

Fig. 3 – XRD pattern of (a) bare and (b) Co-coated $MmNi_{2.38}Al_{0.82}Co_{0.66}Si_{0.77}$ $Fe_{0.13}Mn_{0.24}$ MH alloy.

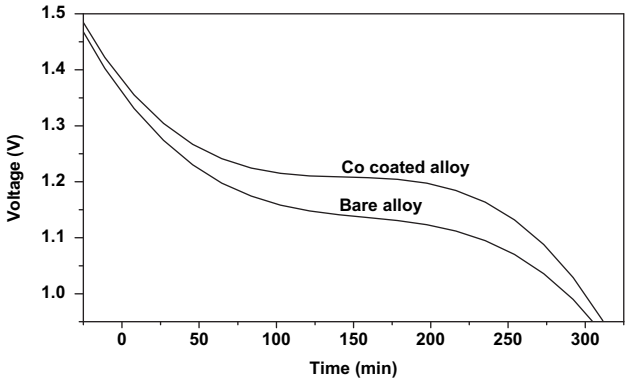

Fig. 4 – Discharge curves of the Ni–MH cell having bare and Co-coated MH electrodes at C/5 rate.

expansion during hydride formation of the alloy. However, elaborate studies on cobalt microencapsulation of metal hydride alloys have not appeared in the literature. In this paper, we present the results of our study on cobalt-microencapsulated $MmNi_{2.38}Al_{0.82}Co_{0.66}Si_{0.77}Fe_{0.13}Mn_{0.24}$ (the best performing alloy with an optimum lanthanum/cerium ratio of 11.65 identified in our previous work [5]) by EIS at different SOCs.

2. Experimental

2.1. *Metal hydride alloy preparation and electroless coating*

Lanthanum-rich non-stoichiometric $MmNi_{2.38}Al_{0.82}Co_{0.66}Si_{0.77}$ $Fe_{0.13}Mn_{0.24}$ hydrogen storage alloy (produced by arc melting at DMRL in collaboration with CECRI) was used for this study. The purity of the constituent elements was above 99 wt.%. The constituent elements were melted together in a button arc-furnace under argon atmosphere (0.5 bar). The samples were re-melted several times by spinning the buttons upside down after each melting to ensure homogeneity. The chunk of the metal hydride alloy was ground for several hours to obtain fine powder.

The alloy powder with a particle size of 75 μm was used for electroless coating. Prior to coating, the alloy was sensitized by immersing in acidified $SnCl_2$ (10 g l^{-1}) for 10 min. Electroless deposition of cobalt was carried out with moderate stirring in an alkaline hypophosphite bath [22] at 90 °C for 30 min.

Table 3 – The lattice parameters and cell volume of $Cacu_5$-type bare and Co-coated MH alloy.

Alloy	Cell parameters		Cell volume (Å^3)
	a(Å)	c(Å)	
Bare MH alloy	5.0502	4.0472	89.39
Co-coated MH alloy	5.0576	4.0590	89.92

The *p*H was monitored continuously and maintained around 9 by periodic addition of NH_4OH. After deposition, the alloy powder was rinsed with deionized water, filtered and dried. The details of bath composition and process variables are presented in Table 1.

2.2. *Physical characterization*

Surface morphology of the bare and coated alloy powders were examined by SEM (Hitachi model S-3000H). Qualitative surface elemental analysis was done with energy dispersive analysis by X-rays (EDAX). The crystal structure was identified by X-ray diffraction using a Bruker D8 Advance equipment.

2.3. *Charge–discharge experiments*

MH electrodes for bare and coated alloys were prepared with 1.0 g samples of alloy powder [5]. A slurry of the alloy powder with appropriate amounts of a conducting material (KS 44) and binder (polytetrafluoroethylene) was applied on both sides of a nickel foam (90% porous) substrate (3 cm × 2 cm). The electrode was pressed under 75 MPa and heat-treated at 408 K for 1 h. The thickness of the electrode after compaction was 1.0 mm. A sintered nickel hydroxide [$Ni(OH)_2$/NiOOH]

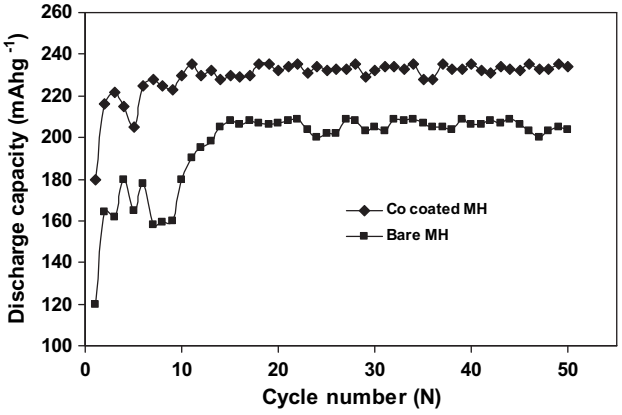

Fig. 5 – Discharge capacity of bare and Co-coated MH electrode at C/5 rate.

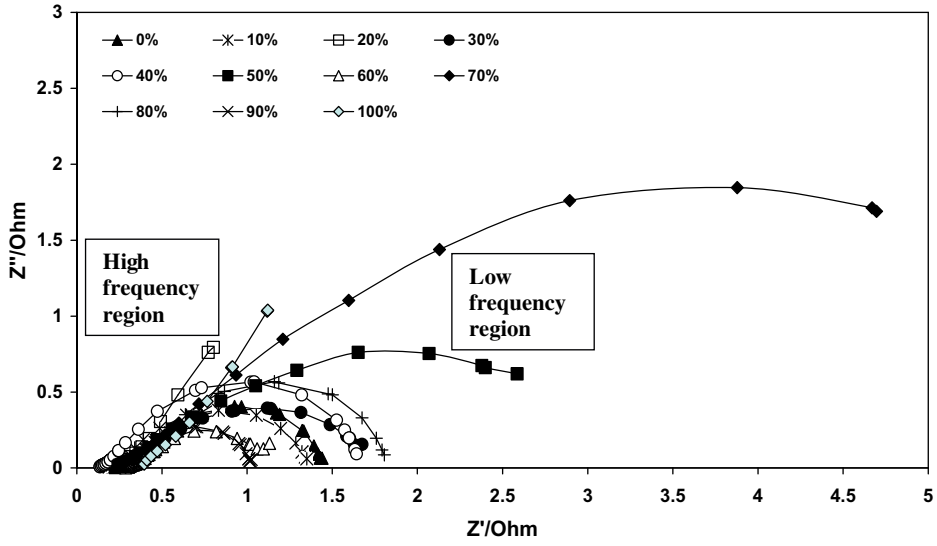

Fig. 6 – Nyquist plots of the EIS of bare MH electrodes at various state-of-charge.

electrode of thickness 1.0 mm was used as the positive electrode. A polyamide non-woven cloth was used as the separator. The negative electrode was sandwiched between two positive electrodes. A 6 M solution of KOH was used as the electrolyte. Galvanostatic charge–discharge cycling and SOC experiments were performed at a current density of 60 mA g^{-1} on a Bitrode model 2-10-12 LCN cycle life tester. Charging was done for 7 h and discharging was done until the potential of the MH electrode reached −0.700 V with respect to an Hg/HgO reference electrode. Life cycling experiments were performed with an overcharge factor of 20% with a 10 min pause after full charge.

2.4. *EIS investigations*

Electrochemical studies of the bare and cobalt-coated MH electrodes were performed in a three-electrode compartment cell with an $Hg/HgO/OH^-$ reference electrode using an Autolab Potentiostat/Galvanostat model 30. Electrochemical impedance spectroscopy experiments were carried out in the frequency range of 100 kHz–10 mHz after activation of the MH electrode at various SOCs. The amplitude of perturbation was 10 mV.

3. Results and discussion

3.1. *Surface characteristics*

The observed surface morphology of the bare and cobalt-coated alloys are illustrated in Fig. 1(a) and (b). From Fig. 1(a) it can be seen that the bare material is a heterogeneous mixture of crystalline alloy particles. Very small particles also may be seen in the cleavages of bare alloy. Fig. 1(b) reveals a uniform coating of cobalt over the alloy particles. The

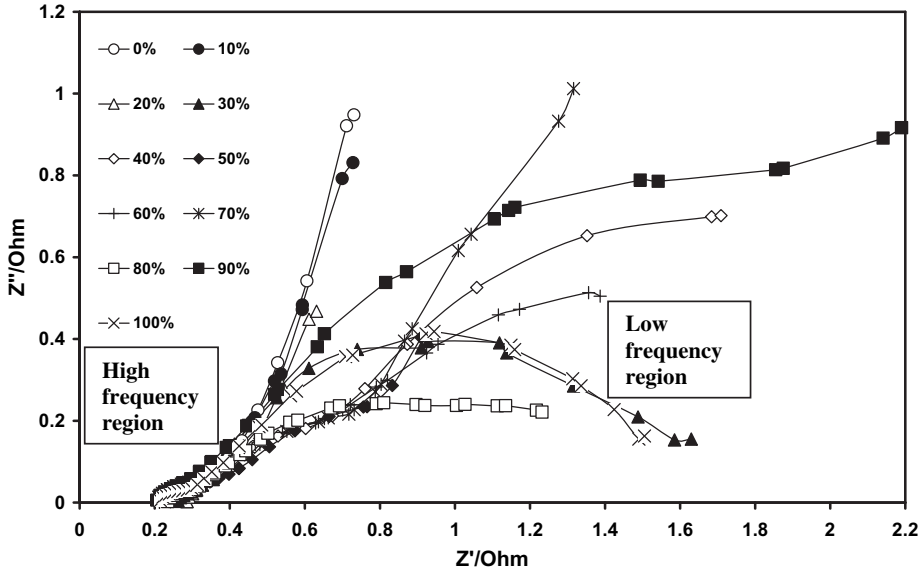

Fig. 7 – Nyquist plots of the EIS of Co-coated MH electrodes at various state-of-charge.

surface of bare alloy appears passivated whereas the cobalt-coated alloy appears smooth with less number of cleavages.

Fig. 2(a) and (b) present the EDAX spectra of the alloy powder before and after cobalt coating. The coated material has nickel and cobalt contents of 31 and 43 wt.%. The elemental compositions of the bare and cobalt-coated alloys are presented in Table 2, which confirms the presence of additional cobalt in the coated powder. The powder X-ray diffraction patterns of the bare and cobalt-coated $MmNi_{2.38}Al_{0.82}Co_{0.66}Si_{0.77}Fe_{0.13}Mn_{0.24}$ alloy are given in Fig. 3. The peaks correspond to JCPDS card no. 25-1136. Both the bare and cobalt-coated MH alloy possess the $CaCu_5$-type hexagonal structure. The lattice parameters and cell volume are presented in Table 3.

3.2. *Weight of the cobalt coating*

Weight measurements of the alloy particles before and after cobalt microencapsulation indicated a weight gain of 20%.

3.3. *Charge/discharge characteristics*

Fig. 4 shows the discharge characteristics of the bare and cobalt-coated alloy electrodes. The profiles of the curves clearly indicate that the voltage of the cobalt-coated alloy electrode is higher throughout the discharge process compared to that of the bare alloy electrode. This suggests that the surface modification of the negative active material can effectively improve the conductivity. In fact, cobalt coatings are known to improve the discharge characteristics and enhance the discharge capacity [22]. The cycling behaviour of the bare and cobalt-coated alloy electrodes are illustrated in Fig. 5. It is evident that the encapsulation imparts a higher discharge capacity and a longer cycle life to the alloy.

3.4. *EIS experiments*

The charge transfer resistance (R_{ct}) [23] was determined from impedance plots using equivalent circuits for the bare and coated electrodes at various SOCs. The exchange current density (I_o) [6] was calculated using the Butler–Volmer equation.

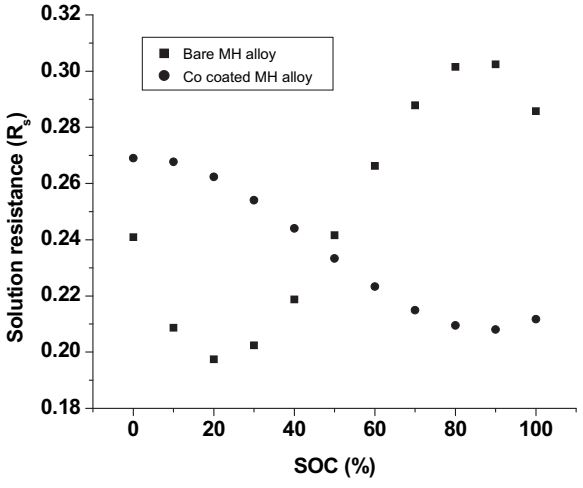

Fig. 8 – Solution resistance of the bare and Co-coated MH electrode at various SOC.

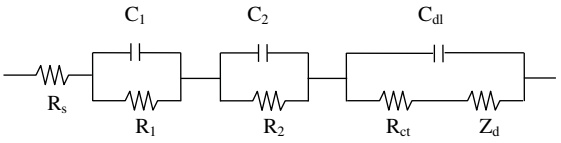

Fig. 9 – Equivalent circuit of Faradaic current response for alloy particles in MH electrode.

The EIS spectra of the bare and cobalt-coated electrodes at various SOCs are depicted in Figs. 6 and 7, respectively. Fig. 6 shows that at most of the values of SOCs studied, the semicircles in the high frequency region are characteristic of the charge transfer reaction at the electrode/electrolyte interface [24]. The high frequency intercepts primarily arise from electrolyte resistance (R_s). The large semicircles in the low frequency region indicate that the relaxation period is distinct at different SOCs. The linearity in the very low frequency region for 20 and 100% SOCs suggests hydrogen diffusion in the bare alloy. The loci have distorted capacitive semicircular arcs at high frequencies and a linear region at low frequencies. The high frequency semicircle in the Nyquist diagram relates to the charge transfer process. The diffusion of hydrogen in the electrode is indicated as a linear part in the lower frequency region. The depression in the semicircle may be due to (i) the surface roughness, (ii) the heterogeneity and (iii) the existence of two different processes with more or less same relaxation times.

The impedance responses of bare and cobalt-coated alloy electrodes show a marked decrease due to cobalt microencapsulation over the frequency range investigated. This is because the cobalt coating, by virtue of its higher conductivity, reduces the charge transfer resistance by acting as an efficient current collector. The resultant reduction in the overpotential during the charge/discharge processes leads to an increase in discharge capacity of the electrode.

Fig. 8 shows R_s of the bare and coated MH electrode at various SOC. For the bare alloy, R_s and R_{ct} increase at most of the SOCs.

Table 4 – Contact resistance and charge transfer resistance values for bare and cobalt-coated MH alloy electrodes at various SOC.

State-of-charge (%)	R_s(Ω)		R_{ct} (Ω)	
	Bare alloy	Co-coated alloy	Bare alloy	Co-coated alloy
0	0.239	0.271	0.051	0.126
10	0.184	0.256	0.072	0.099
20	0.237	0.284	0.086	0.112
30	0.256	0.240	0.092	0.117
40	0.129	0.240	0.093	0.107
50	0.235	0.250	0.095	0.103
60	0.287	0.212	0.108	0.107
70	0.277	0.204	0.105	0.111
80	0.364	0.227	0.110	0.110
90	0.249	0.203	0.111	0.103
100	0.297	0.211	0.120	0.098

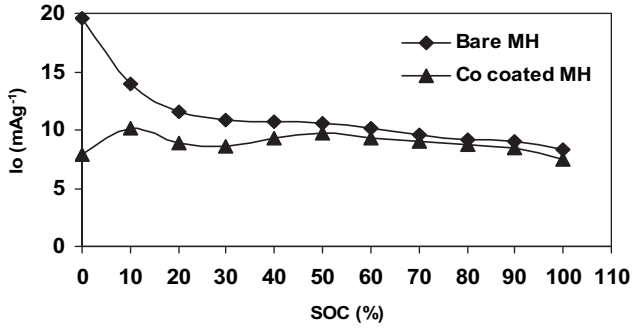

Fig. 10 – Exchange current density of the bare and Co-coated MH electrode at various SOC.

Our results are in agreement with literature reports [25]. However, contribution of R_s to the total impedance is lower in the case of coated alloy electrode. The linearity in the high frequency region at most of the SOCs for the cobalt-coated alloy is indicative of hydrogen diffusion in the bulk of the coated alloy.

The value of R_{ct} was derived by fitting the impedance parameters in the equivalent circuit (Fig. 9) for the MH electrode. The values of R_s and R_{ct} for the bare and cobalt-coated alloy electrodes are presented in Table 4. The value of R_s decreased significantly after surface modification with cobalt. The presence of cobalt on the surface prevents the oxidation of alloy particles and acts as a conductive coating. Consequently, the surface modification decreases R_s between the alloy particles and increases the conductivity of MH electrode. R_{ct} was also found to get reduced after surface modification of the alloy with cobalt.

From Fig. 10 it can be seen that the I_o of the bare alloy varies significantly with SOC. However, for the cobalt-coated alloy I_o varies slightly up to 40% SOC. This is related to a minimal expansion of the lattice at the nickel sites during electrochemical hydrogenation up to 40% SOC. Therefore, we conclude that the cobalt encapsulation helps in the hydriding reaction during the charge transfer process.

The exchange current density of bare alloy electrode is high at low SOCs whereas it remains constant at around 10 mA g^{-1} for SOCs above 40%. The I_o value decreases with an increase in SOC. This suggests that the internal resistance of bare alloy is low at low SOCs, increasing with increasing SOC. However, the internal resistance of cobalt-coated alloy is uniform at all values of SOC.

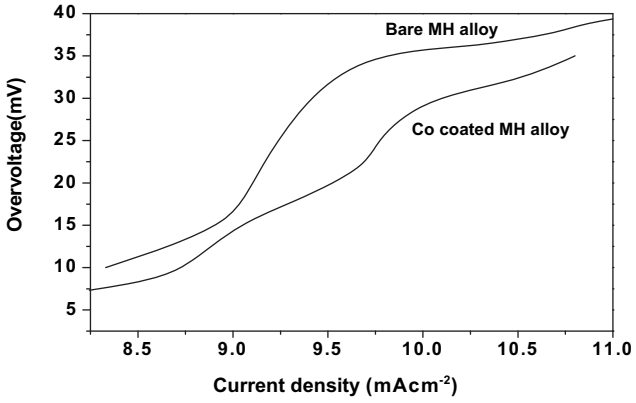

Fig. 11 – Typical linear polarization curves of the bare and Co-coated MH alloy electrode.

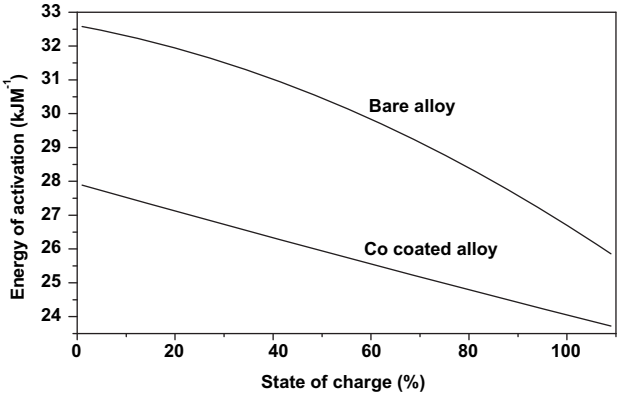

Fig. 12 – Apparent activation energy curves of bare and Co-coated MH alloy at various SOC.

3.5. *Polarization characteristics*

Fig. 11 illustrates the polarization behaviour of the bare and cobalt-coated alloy electrodes. When the overvoltage is perturbed within a small range, the current density variations approximate to a linear region from which the value of I_o was estimated. The polarization plots suggest that the cobalt encapsulation reduces the overvoltage, suggesting that the coating acts as a good current collector.

3.6. *Apparent activation energy*

The apparent activation energy for the dehydriding process was calculated from the plots of exchange current density versus 1/T according to the following equation.

$$E_a = -R(\log\ I_o/1/T)$$

where E_a is the apparent activation energy in kJ $mole^{-1}$ (Fig. 12). Apparent activation energy is the energy that the reactants must possess to facilitate the reactions to occur. The value of E_a is higher for the bare alloy at all SOCs. This suggests that the coated alloy provides an easy path for the hydrogenation/

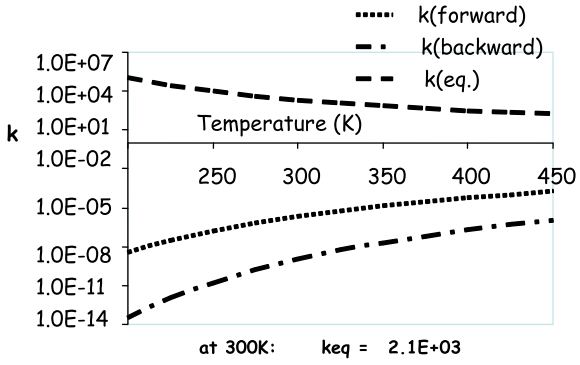

Fig. 13 – Rate constants of the complex formed for the bare MH alloy as a function of temperature.

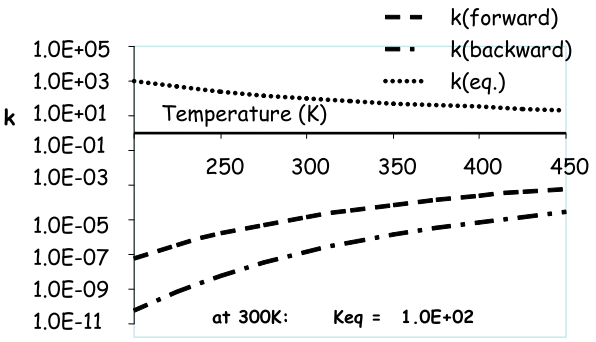

Fig. 14 – Rate constants of the complex formed for the Co-coated MH alloy as a function of temperature.

dehydrogenation reactions. It may be noted that E_a decreases with increasing SOC for both the bare and coated electrodes. At 10% SOC, E_a for the bare and coated alloy are 32.2 and 27.4 kJ mole^{-1}, respectively. However, at 100% SOC, E_a values for the bare coated alloys are 27.2 and 24 kJ mole^{-1}, respectively. It is clear that the cobalt microencapsulation changes the activity of the electrochemical reactions.

Figs. 13 and 14 represent the forward and backward rate constants (k) of the complex formed with the bare and cobalt-coated alloy electrodes. The k-values were calculated with the help of the software Sinex 2006. At 300 K, the equivalent rate constant, k_{eq}, for bare and coated alloys are 2.1×10^3 and 1.2×10^2, respectively. The k_{eq} values suggest the more facile reversibility of the cobalt-coated alloy complex as compared to the bare alloy complex. As a result, the cycle life of the coated alloy electrodes increases.

4. Conclusions

The effect of cobalt microencapsulation on the discharge capacity, cycle life and electrochemical impedance of $MmNi_{2.38}Al_{0.82}Co_{0.66}Si_{0.77}Fe_{0.13}Mn_{0.24}$ alloy electrodes has been investigated. It was found that microencapsulation significantly improved the electrocatalytic activity for hydrogen evolution reaction and reduced the overpotential for charging/discharging, both of which lead to a remarkable increase in electrode capacity and cycle life. The EIS studies at various SOCs for the bare and coated alloy electrodes reveal that the reaction resistance is reduced significantly. The steady exchange current densities of the cobalt-coated alloy electrodes suggest an enhanced catalytic activity, which favors faster reaction rates during charge, discharge and overcharge. Cobalt-coated alloys are also more reversible compared to the bare alloy as they display a lower value of equilibrium constant.

Acknowledgements

The authors thank the Director, CECRI for encouragement and permission to publish this work. Thanks are due to MNES, New Delhi for sanctioning a Grant-In-Aid project on 'Development of Advanced Ni–MH Battery fitted Electric Cycle and Field Studies' in which the above work has been done. The authors also thank Dr. G. Balachandran, DMRL, Hyderabad, India for preparing the MH alloys. One of the authors, GN, thank the Director, CECRI for permission to carry out her M.Sc. project work and KM for guidance.

REFERENCES

[1] Zhang L. Batteries rechargeable, encyclopedia of materials: science and technology. USA: Elsevier Ltd.; 2008. p. 463–483.
[2] Ma S, Gao M, Li R, Pan H, Lei Y. A study on the structural and electrochemical properties of $La_{0.7-x}Nd_xMg_{0.3}Ni_{2.45}Co_{0.75}Mn_{0.1}Al_{0.2}$ ($x = 0.0$–3.0) hydrogen storage alloys. J Alloy Compd 2008;457:457–64.
[3] Ruiz FC, Castro EB, Real SG, Peretti HA, Visintin A, Triaca WE. Electrochemical characterization of AB_2 alloys used for negative electrodes in Ni/MH batteries. Int J Hydrogen Energy 2008;33:3576–80.
[4] Yuan A, Xu N. A study on the effect of nickel, cobalt or graphite addition on the electrochemical properties of an AB_5 hydrogen storage alloy and the mechanism of the effects. J Alloy Compd 2001;322:269–75.
[5] Ananth MV, Raju M, Manimaran K, Balachandran G, Nair LM. Influence of rare earth content on Mm-based AB_5 metal hydride alloys for Ni–MH batteries—an X-ray fluorescence study. J Power Sources 2007;167:228–33.
[6] Tliha M, Mathlouthi M, Lamloumi J, Percheron-Guegan A. Electrochemical kinetic parameters of a metal hydride battery electrode. Int J Hydrogen Energy 2007;32:611–4.
[7] Raju M, Manimaran K, Ananth MV, Renganathan NG. An EIS study on the capacity fades in $MmNi_{3.6}Al_{0.4}Mn_{0.3}Co_{0.7}$ metal-hydride electrodes. Int J Hydrogen Energy 2007;32:1721–7.
[8] Feng F, Northwood DO. Effect of surface modification on the performance of negative electrodes in Ni/MH batteries. Int J Hydrogen Energy 2004;29:955–60.
[9] Chen WX. Cyclic voltammetry and electrochemical impedance of $MmNi_{3.6}Co_{0.7}Mn_{0.4}Al_{0.3}$ alloy electrode before and after treatment with a hot alkaline solution containing reducing agent. J Power Sources 2000;90:201–5.
[10] Li XF, Dong HC, Zhang AQ, Wei YW. Electrochemical impedance and cyclic voltammetry characterization of a metal hydride electrode in alkaline electrolytes. J Alloy Compd 2006;426:93–6.
[11] Liu Y, Pan H, Gao M, Zhu Y, Lei Y, Wang Q. Electrochemical studies on $La_{0.7}Mg_{0.3}Ni_{3.4-x}Co_{0.6}Mn_x$ metal hydride electrode alloys. Mater Chem Phys 2004;84:171–81.
[12] Darowicki K, Slepski P. Instantaneous electrochemical impedance spectroscopy of electrode reactions. Electrochim Acta 2004;49:763–72.
[13] Hammouche A, Karden E, Doneker RWD. Monitoring state-of-charge of Ni–MH and Ni–Cd batteries using impedance spectroscopy. J Power Sources 2004;127:105–11.
[14] Haran BS, Popov BN, White RE. Theoretical analysis of metal hydride electrodes – studies on equilibrium potential and exchange current density. J Electrochem Soc 1998;145:4082–90.
[15] Deng C, Shi P, Zhang S. Effect of surface modification on the electrochemical performances of $LaNi_5$ hydrogen storage alloy in Ni/MH batteries. Mater Chem Phys 2006;98:514–8.
[16] Wei X, Zhang P, Dong H, Liu Y, Zhu J, Yu G. Electrochemical performances of a Co-free $La(NiMn\ AlFe)_5$ hydrogen storage alloy modified by surface coating with Cu. J Alloy Compd 2008;458:583–7.
[17] Naito K, Matsunami T, Okuno K, Matsuoka M, Iwakura C. Electrochemical characteristics of hydrogen storage alloys modified by electroless nickel coatings. J Appl Electrochem 1994;24:808–13.
[18] Jenq SN, Yang HW, Wang YY, Wan CC. Modification of $Ti_{0.35}Zr_{0.65}Ni_{1.2}V_{0.6}Mn_{0.2}$ alloy powder by electroless nickel

coating and its influence on discharge performance. J Power Sources 1995;57:111–8.
[19] Shan X, Payer JH, Wainright JS. Increased performance of hydrogen storage by Pd-treated $LaNi_{4.7}Al_{0.3}$, $CaNi_5$ and Mg_2Ni. J Alloy Compd 2006;426:400–7.
[20] Chartouni D, Meli F, Zuetell A, Gross K, Sclapbach L. The influence of cobalt on the electrochemical cycling stability of $LaNi_5$-based hydride forming alloys. J Alloy Compd 1996;241:160–6.
[21] Sakai T, Yoshinaga H, Miyamura H, Kuriyama N, Ishikawa H. Rechargeable hydrogen batteries using rare-earth-based hydrogen storage alloys. J Alloy Compd 1992;180:37–54.
[22] Law HH, Vyas B, Zahurak SM, Kammlott GW. A novel plating process for microencapsulating metal hydrides. J Electrochem Soc 1996;143:2596–601.
[23] Raju M, Ananth MV, Vijayaraghavan L. Influence of temperature on the electrochemical characteristics of $MmNi_{3.03}Si_{0.85}Co_{0.60}Mn_{0.31}Al_{0.08}$ hydrogen storage alloys. J Power Sources 2008;180:830–5.
[24] Wang LB, Wang JB, Yuan HT, Wang YJ, Li QD. An electrochemical investigation of $Mg_{1-x}Al_xNi$ ($0 \leq x \leq 0.6$) hydrogen storage alloys. J Alloy Compd 2004;385:304–8.
[25] Durairajan A, Haran BS, Bopov BN, White RE. Cycle life and utilization studies on cobalt microencapsulated AB_5 type metal hydride. J Power Sources 1999;83:114–20.